Chemical Physics Letters 508 (2011) 125–129

Contents lists available at ScienceDirect

Chemical Physics Letters

journal homepage: www.elsevier.com/locate/cplett

Control of spectroscopic fluorescence parameters of Nd^{3+} ions as a function of concentration in a SiO_2–Na_2O–Al_2O_3–B_2O_3 glass system

E.O. Serqueira [a], N.O. Dantas [a], M.J.V. Bell [b,*]

[a] Laboratório de Novos Materiais Isolantes e Semicondutores (LNMIS), Instituto de Física, Universidade Federal de Uberlândia, 38400-902 Uberlândia, MG, Brazil
[b] Grupo de Espectroscopia de Materiais, Departamento de Física, Universidade Federal de Juiz de Fora, 36036-330 Juiz de Fora, MG, Brazil

ARTICLE INFO

Article history:
Received 30 June 2010
In final form 6 April 2011
Available online 9 April 2011

ABSTRACT

Experimental evidence of spectroscopic parameter control was observed in Nd^{3+} ions embedded in a SiO_2–Na_2O–Al_2O_3–B_2O_3 glass system. The parameters $\Omega_{2,4,6}$ and others were determined by the Judd–Ofelt theory. It was found that these parameters were strongly dependent on Nd^{3+} concentration, indicating a ligand field change. This Letter will present and discuss possible mechanisms responsible for changes in the Judd–Ofelt parameters. Furthermore, non-radiative energy transfer mechanisms such as energy migration, cross relaxation and losses from networked phonons and OH^- radicals, will be proposed to explain the observed decrease in $^4F_{3/2} \rightarrow {}^4I_{11/2}$ transition lifetime of Nd^{3+}.

1. Introduction

Glass systems doped with rare-earth (RE) ions have attracted great research interest because of their applications in optical systems [1–3]. In particular, Nd^{3+} ions in certain hosts, depending on their spectroscopic properties, are highly efficient for photonic device applications like laser active media [4], optical amplifiers [5], microchips [6] and planar waveguides [3,7–9].

Among the possible glass compositions, SNAB glass has been proposed as a host for quantum dots and rare earth ions, for optical applications. SNAB glasses result from the combination of network-forming oxides SiO_2 and B_2O_3 together with the network modifier oxide Na_2O and intermediate oxide, Al_2O_3. SiO_2 is transparent in the optical window, B_2O_3 increases the glass transparence. Na_2O reduces the melting point and facilitates the homogenization of the glass system, reducing defects and bubbles. Al_2O_3 is added to increase the chemical resistance and mechanical properties. Previous works reported in the literature have demonstrated that SNAB glassy host favors the growing and control of the magneto-optic properties of semiconductor (CdS [10], CdSSe [10], CdSe [10], PbS [11], PbSe [12,13]) and semi-magnetic (CdMnS [14], PbMnS [15], PbMnSe [16]) quantum dots. Besides, SNAB glass is currently been investigated for co-doping with semiconductor quantum dots and rare earth ions. [17] Potential applications are related to optical devices such as lasers, optical amplifier in the optical window, host of detectors in the visible range (quantum dots of CdS, CdSe, CdSSe) and near infrared (PbS, PbSe), as well as semimagnetic quantum dots that are of interest in sprintronics and quantum computation.

The Judd–Ofelt theory has been of fundamental importance in the quantitative analysis of the spectroscopic properties of RE ions [18–22]. This theory allows Judd–Ofelt parameters Ω_λ ($\lambda = 2, 4, 6$) to be determined which in turn can be used to estimate optical parameters like spontaneous emission probability, branching ratio, emission cross-section, radiative lifetime, quantum efficiency and effective linewidth. These parameters can be used to predetermine if an RE ion host material is favorable for optical device applications.The main objective of this research was to control the spectroscopic parameters of fluorescence of Nd^{3+} ions embedded in a SiO_2–Na_2O–Al_2O_3–B_2O_3 glass system as a function of Nd^{3+} concentration. The SiO_2–Na_2O–Al_2O_3–B_2O_3 glass system was chosen as host because it is transparent in the electromagnetic spectrum range from ultraviolet (UV) to near infrared (NIR) where the main permitted electronic transitions of Nd^{3+} ion absorption and emission occur [14,18,23,24]. Electric and magnetic dipole transitions are permitted due to the wave function mix of the parity states opposed to the $4f^N$ configuration of rare earth ions. According to the Judd–Ofelt Theory, electric dipole oscillator strength, between initial $|f^n[\alpha SL]J\rangle$ and final states $|f^n[\alpha' S' L']J'\rangle$, can be expressed as

$$f^{ED}(J,J') = \frac{8\pi^2 mc}{3h} \times \frac{E}{(2J+1)}\chi \sum_{\lambda=2,4,6} \Omega_\lambda \left|\left\langle f^n[\alpha SL]J \right|\left| U^{(\lambda)} \right|\left| f^n[\alpha' S' L']J' \right\rangle\right|^2, \quad (1)$$

where m is electron mass, c the speed of light, E the transition wave or energy number, h Planck's constant, J the angular moment of the initial state $|f^n[\alpha SL]J\rangle$, $\chi = (n^2+2)^2/9n$ the central field correction factor, n the refraction index at the wave number ε, Ω_λ the Judd–Ofelt intensity parameter and $\left|\left\langle f^n[\alpha SL]J||U^{(\lambda)}||f^n[\alpha' S' L']J' \right\rangle\right|^2$ represents the reduced matrix elements of the tensor operator U^λ

* Corresponding author.
E-mail address: mjbell@fisica.ufjf.br (M.J.V. Bell).

0009-2614 © 2011 Elsevier B.V. Open access under the Elsevier OA license.
doi:10.1016/j.cplett.2011.04.034

In this case, quadrupole oscillator strength is negligible [25].The Judd–Ofelt intensity parameters, $\Omega_\lambda \quad (\lambda = 2, 4, 6)$ can be obtained from experimental oscillator strength given by

$$f^{\exp}(\lambda) = \frac{mc}{\pi e^2 N}\int \alpha(\lambda)d\lambda \tag{2}$$

where N is the RE ion concentration per unit volume (ions/cm^3) and $\alpha(\lambda)$ the absorption coefficient of wavelength λ. According to the Judd–Ofelt Theory selection rule, experimental oscillator strength ($f^{\exp}$) can be expressed as $f^{\exp} = f^{ED} + f^{MD}$, when there are magnetic dipole transitions (f^{MD}).

Radiative transition rates (A) can be obtained by the expression

$$A(J,J') = \frac{64\pi^4 e^2}{3h(2J+1)\lambda^3}\chi\sum_{\lambda=2,4,6}\Omega_\lambda\left|\left\langle f^n[\alpha SL]J\right|\left|U^{(\lambda)}\right|\left|f^n[\alpha' S'L']J'\right\rangle\right|^2. \tag{3}$$

The emission branching ratio for transitions originating from initial manifold can be obtained from the radiative transition probabilities $A(J,J')$ using the following equation [26]:

$$\beta\left({}^4F_{3/2} \rightarrow {}^4I_{J'}\right) = \frac{A\left({}^4F_{3/2} \rightarrow {}^4I_{J'}\right)}{\sum_{J'} A\left({}^4F_{3/2} \rightarrow {}^4I_{J'}\right)}, \tag{4}$$

where the summation includes each J' (J' = 9/2, 11/2, 13/2 and 15/2).

To compare theoretical data obtained from Eq. (4) with experimental data, the ratio of the integral of an emission band, $\int I(\lambda)d\lambda$, to the sum of the integrals of all emission bands, $\sum\int I(\lambda)d\lambda$ is calculated. This results in the experimental emission branching ratio and is represented by

$$\beta_{\exp} = \frac{\int I(\lambda)d\lambda}{\sum\int I(\lambda)d\lambda}. \tag{5}$$

The spontaneous emission cross-section between ${}^4F_{3/2} \rightarrow {}^4I_{J'}$, where the fluorescence lifetime (τ) was measured, is represented by [26,27]

$$\sigma_{em}\left({}^4F_{3/2} \rightarrow {}^4I_{J'}\right) = \frac{\lambda_p^4}{8\pi c n \Delta\lambda_{eff}}A\left({}^4F_{3/2} \rightarrow {}^4I_{J'}\right), \tag{6}$$

where λ_p is the peak emission wavelength, c the speed of light in a vacuum, n the refractive index at each emission peak wavelength and $\Delta\lambda_{\text{eff}}$ the effective linewidth. This is used instead of the full-width at half-maximum linewidth because the emission band is asymmetric. It is characterized in the name of an effective linewidth as below [26,27]

$$\Delta\lambda_{eff} = \frac{\int I(\lambda)d\lambda}{I_{\max}} \tag{7}$$

where $I_{\max}$ is the maximum intensity at fluorescence emission peaks.

2. Experimental details

Two sets of SNAB matrices with nominal composition $40SiO_2{\cdot}30Na_2O{\cdot}1Al_2O_3{\cdot}29B_2O_3$ (mol%) were synthesized by the fusion method. These were un-doped and doped with Nd^{3+} ions, resulting in templates labeled SNAB and SNAB + XNd_2O_3 (wt.%), respectively. Powder was melted at 1300 °C for 15 min in a carbon rich atmosphere using porcelain crucibles in which the melt was subjected to rapid cooling. The optical absorption spectra (OA) were obtained using a SHIMADZU UV-3600 spectrophotometer, photoluminescence (PL) and time-resolved photoluminescence (TRPL) spectra where the samples were excited by a He-Cd laser, λ_{exc} = 325 nm, and collected by a photomultiplier that detects photons from 350 to 900 nm. All measurements were taken at room temperature.

3. Results and discussion

Figure 1 shows the optical absorption spectra of the SNAB glass matrix both un-doped and doped with $5Nd_2O_3$ (wt.%) and the fluorescence spectrum of the Nd^{3+} ions embedded in a glassy host doped with $5Nd_2O_3$ (wt.%). Based on the literature [23], it was possible to identify the OA bands and from them obtain the energy level values of the Nd^{3+} ions embedded in the SNAB glassy host. It was observed that the optical gap of the SNAB glass matrix was relatively large which enabled observation of the allowed electron transitions of the higher energy Nd^{3+} ions (e.g. ${}^4I_{9/2} \rightarrow {}^2D_{5/2}$) corresponding to a band centered at about 350 nm (28571 cm^{-1}).

Figure 2 shows the behavior of the Ω_2, Ω_4, Ω_6 JO parameters and Ω_6^{-1} as a function of the concentration of Nd^{3+} ions embedded in the SNAB glass. It is important to note that even though the use of Judd–Ofelt theory is usually restricted to the calculation of $\Omega_{2,4,6}$ parameters when the Rare Earth concentration is low (which means that such concentration would not interfere in the glass structure), it can be used when concentrations of Rare Earth ions may have influence in the glass itself [28–31].

It was observed that Ω_2 increased from 0.8 to 1.7 $\times$ 10^{-20} cm^2 as a function of Nd_2O_3 concentration up to X = 3.0. Above this value, the Ω_2 parameter is constant. The behavior of the Ω_6 parameter is similar to that of Ω_2 while Ω_4 remains practically constant throughout the concentration range. In all cases, the following relationship was observed $\Omega_4 > \Omega_2 > \Omega_6$.

According to the literature, Ω_2 is usually related to the dependence of the covalency between RE^{3+} ions and ligand anions and the asymmetry of the local environment around the site of RE^{3+}. Thus, the lower the value of Ω_2 is, the more centrosymmetric the ion site is and the more ionic the ligand chemical bonds are [21,24,32–37]. Another interpretation for the behavior of Ω_2 could come from structural changes in the glass due to the moderately high RE concentrations. According to the Judd–Ofelt theory, these phenomenological parameters are given by [18,19]:

$$\Omega_t = (2t+1)\sum_{p,s}|A_{s,p}|\Xi(s,t)(2s+1) \tag{8}$$

where the two main contributions to the $\Omega(t)$ parameters arise from the $A_{s,p}$ and Ξ terms. The $A_{s,p}$ term is associated with the Crystal Field parameters of rank s with the pth component being related to structural changes in the vicinity of the rare earth ions; it is expressed by the following relation [18,19]

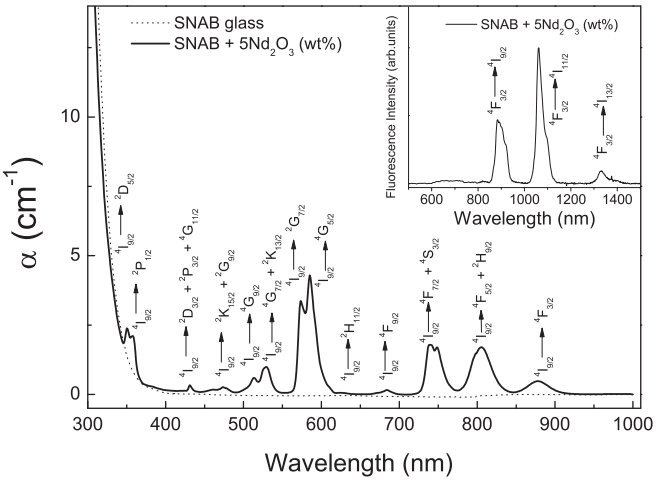

Figure 1. Optical absorption spectra of the SNAB glass matrix un-doped and doped with 5 Nd_2O_3 (wt.%) and the fluorescence spectra of Nd^{3+} ions embedded in the SNAB glass matrix doped with 5 Nd_2O_3 (wt.%).

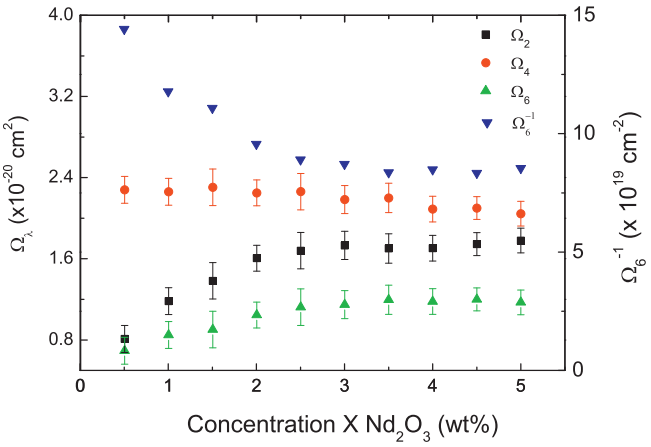

Figure 2. Behavior of $\Omega_{2,4,6}$, Judd–Ofelt parameters and $1/\Omega_6$ in function of the Nd_2O_3 concentration in the SNAB glass matrix.

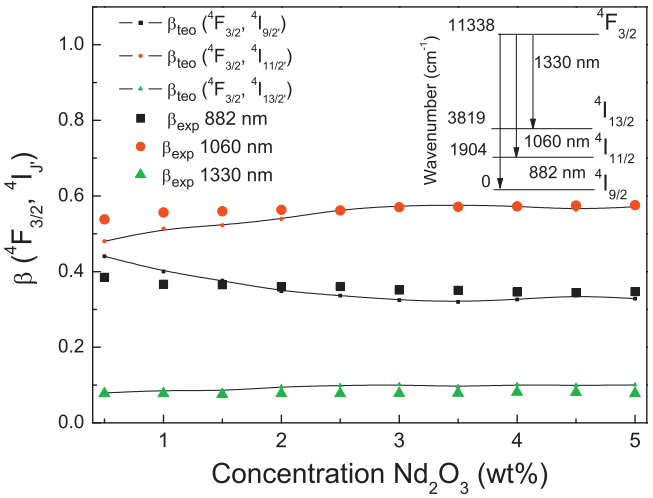

Figure 3. Branching ratio (β_{teo}), obtained by Judd–Ofelt calculations and experimental branching ratio (β_{exp}), obtained from fluorescence measurements as a function of increasing concentrations of Nd_2O_3 embedded in a SNAB glass matrix.

Table 1
Judd–Ofelt parameters ($\Omega_\lambda \times 10^{-20}$ cm^2) of Nd^{3+} ions in different hosts.

Host	Ω_2	Ω_4	Ω_6	Reference
CANB glass	4.40	5.20	2.70	[41]
CANS glass	3.70	5.00	2.90	[41]
ED-2	3.30	4.68	5.18	[41]
LSCA	3.34	4.42	2.02	[41]

$$A_{s,p} = (-1)^p[(s-p)!/(s+p)!]^{1/2}\sum_n g_n \frac{e^z}{r_n^{z+1}} P_z^p \cos(\phi_n)\exp(-ip\theta_n) \quad (9)$$

parameters g_n are the ligand charges located at the position (r_n, φ_n, θ_n) in spherical coordinates with respect to the position of RE ions. According to this expression, the radial distribution of the rare earth inside the site is dominant to the lower s parameter.

In this study, Ω_2 increased as a function of Nd_2O_3 concentration in the SNAB glass matrix. In this way the behavior of Ω_2 may be related to Nd^{3+} cluster formation or assuming that breaks in Nd^{3+} ion bonds resulted in diminished covalency.

The literature [38,39] shows that $1/\Omega_6$ is proportional to the ionicity of the ion in the ligand field. In other words, the greater $1/\Omega_6$ is, the more ionic and fewer covalent bonds the ion will have in the sample. Figure 2 shows that $1/\Omega_6$ behavior is dependent on Nd_2O_3 concentration in the SNAB glass matrix. It was observed that $1/\Omega_6$ decreases with increases in concentration. In other words, Nd^{3+} ionicity decreases in the ligand field with Nd_2O_3 concentration in the glassy host. However, an increase in concentration modifies the crystal field potential by breaking symmetry around and increasing covalency of an ion.

Table 1 shows the JO ($\Omega_\lambda \times 10^{-20}$ cm^2) parameters of Nd^{3+} ions in different hosts. A comparison of the calculations obtained from the JO parameters with those from the table shows that the Nd^{3+} ions in the SNAB glass matrix, with a low concentration of Nd_2O_3, are the more symmetric and less covalent.

The literature [40] also shows that Ω_6 is proportional to host rigidity. In this study, the SNAB matrix embedded with Nd^{3+} ions was less rigid than the samples in Table 1.

Interestingly, most glass types that have been studied (including bismuth borate, calcium aluminum silicate, sodium lead borate, potassium borate, sodium potassium mixed alkali phosphate [30] and oxyfluoride glass ceramics [31]) demonstrate decreases in Ω_2 and Ω_6 parameters with increases in Nd^{3+} concentration. Consequently, these glasses have reduced spontaneous emission rates and increased lifetimes for transitions starting from the $^4F_{3/2}$ level. Reference [28] reports a variation of the Judd–Ofelt parameters in a borosilicate glass with composition similar to the present SNAB glass, where similar trends were observed: Ω_2 changed from 6.26 to 4.14×10^{-20} cm^2, Ω_4 was from 2.39 to 3.25×10^{-20} cm^2 and Ω_6 from 2.49 to 3.07×10^{-20} cm^2, when the concentration of the Rare Earth ion (Tb^{3+}) was from 5 to 20 wt.%.

Figure 3 shows the dependence of the branching ratio (β_{teo}), obtained from Eq. (4) for the $^4F_{3/2} \rightarrow {}^4I_{J'}$ transitions and the experimental branching ratio (β_{exp}) of the PL spectra determined by Eq. (5), on the concentration of Nd_2O_3 embedded in the SNAB glass matrix. From this, it can be seen that the theoretical and experimental behavior of the branching ratios are in strong agreement which suggests that the Judd–Ofelt calculations are valid.

Figure 4 shows the dependence of fluorescence lifetime (τ_{exp}) and radiative lifetime (τ_{rad}) of the Nd^{3+} ion $^4F_{3/2}$ states, on increasing concentrations of Nd_2O_3. There is a significant decrease in τ as Nd_2O_3 concentrations increase. To analyze this dependence, Stokowski [41,42] determined a relationship between experimental lifetime and the concentration of RE^{3+} ions represented by the following expression

$$\tau_{exp} = \frac{\tau_0}{1 + (\frac{N}{Q})^n}, \quad (10)$$

where τ_0 is the lifetime for a diluted system, (N) the concentration of RE ions, and Q the quenching concentration. Q is defined as the concentration at which lifetime is reduced by half. For Nd^{3+} doped glasses, n equals 2 when quenching fluorescence is dominated by cross-relaxation processes. The higher the Q value, the lower the fluorescence of quenching thus resulting in an efficient optical system (e.g. CASM glass [41] with $Q = 5.25 \times 10^{20}$ ions/cm^3). In this study, $Q = 6.08$ Nd_2O_3 (wt.%) (or 5.09×10^{20} ions/cm^3) and $n = 1.09$ were obtained. This means that the SiO_2–Na_2O–Al_2O_3–B_2O_3 glass system is of similar quality to CASM glass and its decrease in lifetime is not dominated by the cross-relaxation phenomenon.

For comparison, the inset of Figure 4 shows the radiative lifetime (τ_{rad}) obtained using the JO Theory. Since this theory assumes that all transitions involved in the calculations are radiative, it can be concluded that the $^4F_{3/2} \rightarrow {}^4I_{9/2}$, $^4F_{3/2} \rightarrow {}^4I_{11/2}$, $^4F_{3/2} \rightarrow {}^4I_{13/2}$ transitions demonstrate increases in spontaneous emission as Nd^{3+}

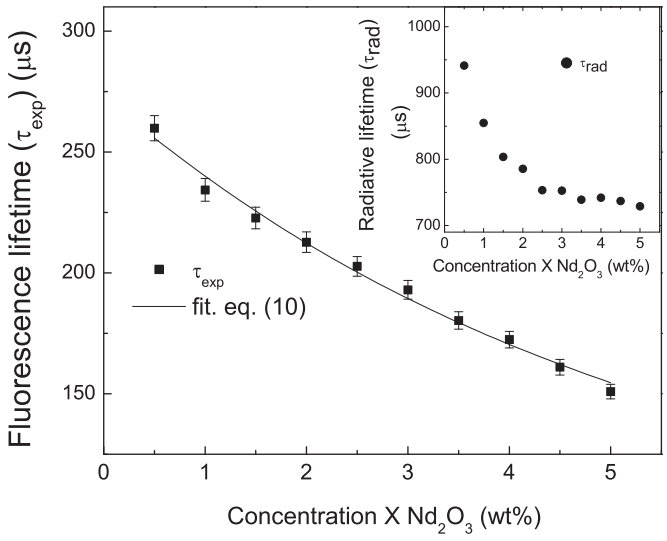

Figure 4. Dependence of the $^4F_{3/2}$ Nd^{3+} state fluorescence lifetime (τ_{exp}) and radiative lifetime (τ_{rad}) (inset) obtained using the Judd–Ofelt Theory as a function of increasing concentrations of Nd_2O_3.

concentration increases. This increase is attributed to a change in the chemical environment around the Nd^{3+} ions which results in a lifetime reduction of the $^4F_{3/2}$ state. A comparison between the radiative lifetimes obtained by Judd–Ofelt and fluorescence also indicates that the quantum efficiency (defined as the τ_{exp}/τ_{rad} ratio) is 25% regardless of Nd^{3+} concentration. Thus, several factors may be directly responsible for the decrease in the $^4F_{3/2}$ lifetime of the Nd^{3+} ions when inserted in the SNAB glass matrix such as: (a) relatively high Nd^{3+} ion concentration causing cross-relaxation (b) hydroxyl presence in the SNAB glassy host of neodymium ions, causing energy transfer between Nd^{3+} and OH^-) high energy phonons of the SNAB glass absorbing part of radiative transitions.

According to the Stokowski model [41,42], the lifetime reduction mechanism, as a function of Nd_2O_3 concentration, is not dominated by the cross-relaxation process. However, the other processes are also confirmed by several researchers [43–48]. They explain the differences in results with two arguments: first, because OH^- radicals are present in the compositions and are considered one of the most important sources of 'quenching' [43–48] and second because of the high phonon energy of the host matrix [43–45]. However, in the low Nd concentration limit, the main mechanisms responsible for the low quantum efficiency should be related with multiphonon decay and OH^- quenching.

Infrared absorption and Raman scattering measurements were performed to further investigate these hypotheses. Figure 5a shows the far infrared spectra of SNAB glass doped with different concentrations of Nd_2O_3. From this, there appears to be strong absorption at about 2790 nm (3584 cm^{-1}) which is characteristic of OH^- radicals [49]. In addition, it can be seen that the concentration of these radicals is almost independent of Nd_2O_3 concentration.

OH^- presence in the SNAB glass matrix can result in an energy transfer caused by non-radiative electronic transitions of Nd^{3+} ions resulting in a reduction in fluorescence lifetime of the $^4F_{3/2}$ state as shown in Figure 4. This energy transfer mechanism can be explained by assuming that the $^4F_{3/2} \rightarrow {}^4I_{9/2}$ and $^4F_{3/2} \rightarrow {}^4I_{13/2}$ transitions of Nd^{3+} ions may occur through non-radiative relaxations associated with the excitation of three and two OH^- phonons, respectively. Energy migration followed by quenching in OH^- results in lifetime reduction as shown in the inset of Figure 5a.

For comparison, Figure 5 shows the Raman spectra of SNAB glass undoped and doped with $2Nd_2O_3$ (wt.%). The Raman spectrum of powder Nd_2O_3 is also shown. The SNAB glass spectra show

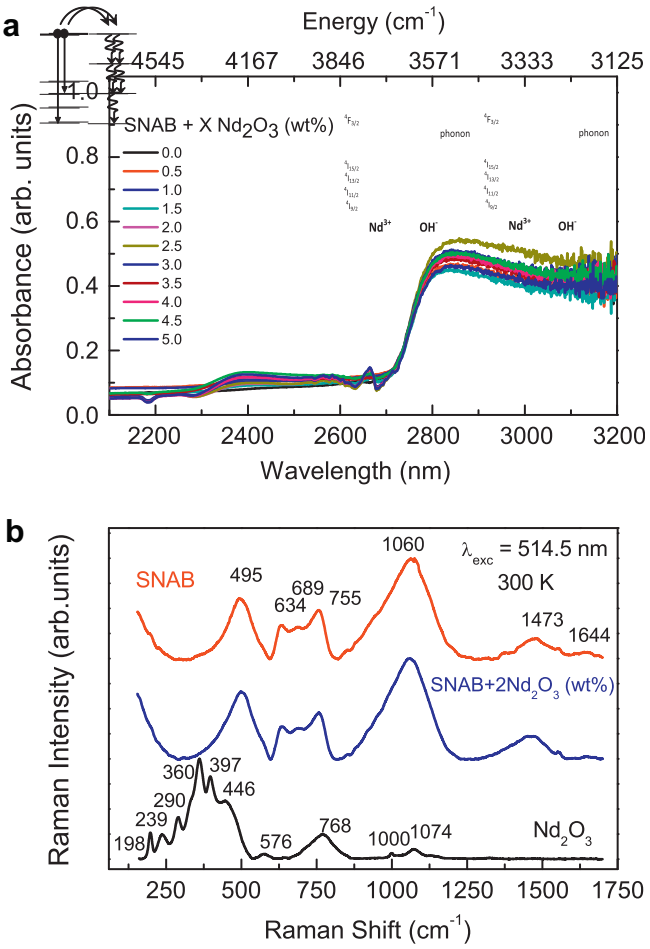

Figure 5. (a) Infrared absorption spectra of SNAB glass doped with different concentrations of Nd_2O_3 in the range 2200–3200 nm (4545–3125 cm^{-1}). The inset displays non-radiative energy transfer processes $^4F_{3/2} \rightarrow {}^4I_{9/2}$ and $^4F_{3/2} \rightarrow {}^4I_{13/2}$ of Nd^{3+} ions for vibrational modes of OH^- radicals. (b) Raman spectra: SNAB, SNAB + $2Nd_2O_3$ (wt.%) and Nd_2O_3.

vibration modes with maximum energy at about 1060 cm^{-1}. The Nd_2O_3 Raman spectra indicate that the energy difference between the Nd^{3+} interest levels also coincides with SNAB glass phonon energy.

In Figure 5b it can be seen that the maximum phonon energy for the SNAB glass matrix is 1060 cm^{-1}. While the energy differences for the $^4F_{3/2} \rightarrow {}^4I_{9/2}$ (11338 cm^{-1} (882 nm)), $^4F_{3/2} \rightarrow {}^4I_{11/2}$ (9434 cm^{-1} (1060 nm)) and $^4F_{3/2} \rightarrow {}^4I_{13/2}$ (7519 cm^{-1} (1330 nm)) transitions are 11, 9 and 7 phonons, respectively (Figure 1). Thus, the $^4F_{3/2} \rightarrow {}^4I_{9/2}$ (11338 cm^{-1} (882 nm)), $^4F_{3/2} \rightarrow {}^4I_{11/2}$ (9434 cm^{-1} (1060 nm)) and $^4F_{3/2} \rightarrow {}^4I_{13/2}$ (7519 cm^{-1} (1330 nm)) transitions can facilitate multi-phonon energy transfer to the Nd^{3+} ion SNAB glass host.

It is well known the multiphonon relaxation rate is given by [50]

$$W_{MP}(T) = C_p \exp[-\alpha \Delta E](1 - \exp(\hbar\omega/kT]^{-p} \quad (11)$$

where C_p and α are nonradiative parameters which depend on the host material, ΔE represents the energy gap between two successive levels, and $p = \Delta E \hbar\omega$ is the number of phonons emitted in the relaxation process. The multiphonon emission process from the $^4F_{3/2}$ level to the $^4I_{11/2}$ level ΔE = 9434 cm^{-1} requires multiple phonon emissions of about 9 phonons because the maximum phonon energy in SNAB glass is 1060 cm^{-1}. In this way, the multiphonon relaxation rate for the $^4F_{3/2}$ level is expected to be very small. The shorter experimental lifetime for the all the samples would mainly

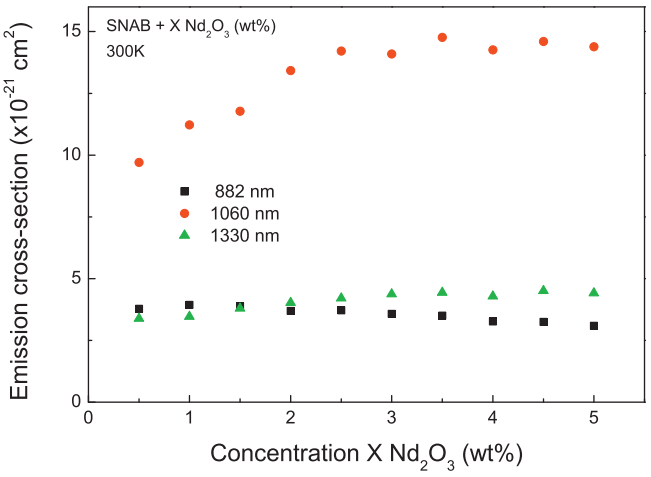

Figure 6. Emission cross section dependence on the transition of the Nd^{3+} ion $^4F_{3/2}$ state to the $^4I_{9/2,11/2,13/2}$ state as a function of the increasing concentration of Nd_2O_3 embedded in the SNAB glass matrix.

be due to excited energy migration among the Nd^{3+} ions, followed by energy transfer to unintentionally introduced impurities and/or defects near to Nd^{3+} ions.

Considering the non radiative processes from the $^4F_{3/2}$ Nd^{3+} level, namely resonant energy migration processes between Nd^{3+} ions (cross relaxation), it can be seen that resonance only occurs for the $^4F_{3/2}$, $^4F_{3/2} \rightarrow {}^4G_{7/2} + {}^2K_{13/2,}$ $^4I_{13/2}$ Nd–Nd interactions. In this case, energy migrates to a neighboring Nd ion and it is excited in the $^4F_{3/2}$ state which favors the $^4F_{3/2} \rightarrow {}^4G_{7/2} + {}^2K_{13/2}$ transition permitted by the JO Theory. The other $^4F_{3/2}$, $^4F_{3/2} \rightarrow {}^4G_{9/2} + {}^2K_{15/2,}$ $^4I_{11/2}$ and $^4F_{3/2}$, $^4F_{3/2} \rightarrow {}^4P_{1/2,}$ $^4I_{9/2}$ cross relaxations are not resonant processes. This can explain the fact that cross relaxation is not a dominant process (since an exponent of about $n = 1$ was obtained for the fit of Eq. (10)).

Figure 6 shows the dependence of emission cross section, obtained from Eq. (6) on the transition of Nd^{3+} ions embedded in the SiO_2–Na_2O–Al_2O_3–B_2O_3 glass system from the $^4F_{3/2}$ state to the $^4I_{9/2}$, $^4I_{11/2}$ and $^4I_{13/2}$ states, as a function of increasing Nd_2O_3 concentration. It can be seen that the $^4F_{3/2} \rightarrow {}^4I_{11/2}$ transition cross section increases with Nd_2O_3 concentration. The $^4F_{3/2} \rightarrow {}^4I_{9/2}$ transition cross section decreases and $^4F_{3/2} \rightarrow {}^4I_{13/2}$ tends to increase starting at concentrations of 1.5 Nd_2O_3 (wt.%).

4. Conclusions

In conclusion, Nd^{3+} ions embedded in a SiO_2–Na_2O–Al_2O_3–B_2O_3 glass system were synthesized by the fusion method. Their optical properties were studied by optical absorption, photoluminescence, Raman and lifetime measurements. Judd–Ofelt parameters, radiative rates, lifetime, branching ratios and emission cross section were calculated. In this study, the SiO_2–Na_2O–Al_2O_3–B_2O_3 glass system with increasing concentrations of Nd_2O_3 produced JO parameters that were dependent on Nd_2O_3 concentration (wt.%).

It was found that these parameters predict emission cross-section increases around 1060 nm and 1330 nm. A reduction in experimental lifetime of the $^4F_{32} \rightarrow {}^4I_{11/2}$ transition with increasing Nd^{3+} concentration was also observed. This was attributed to energy migration, cross relaxation and phonon losses from the network and OH^- radicals.

It was also concluded that both cross relaxation and vibrational modes (glass network and OH^-) contribute to lifetime decreases of the $^4F_{3/2}$ Nd^{3+} level.

The possibility of controlling radiative system parameters, (e.g. the cross section of stimulated emissions at 1060 and 1330 nm transitions, Nd^{3+} ions embedded in the SiO_2–Na_2O–Al_2O_3–B_2O_3 glass system) is attractive for near infrared photonic device applications.

Acknowledgement

The authors would like to thank the following Brazilian organizations for their financial support: CNPq, CAPES and FAPEMIG.

References

[1] J.A. Moon, D.T. Schaafsma, Fiber Integrat. Opt. 19 (2000) 201.
[2] J.S. Sanghera, I.D. Aggarwal, J. Non-Cryst. Solids 256–257 (1999) 6.
[3] R.R. Gonçalves, J.J. Guimarães, J.L. Ferrari, L.J.Q. Maia, S.J.L. Ribeiro, J. Non-Cryst. Solids 354 (2008) 4846.
[4] R.J. Reeves, C. Polley, J.C. Choi, J. Lumin. 129 (2009) 1673.
[5] A. Mussot, Le Parquier, B. Berrier, M. Perard, P. Szriftgiser, Opt. Commun. 282 (2009) 988.
[6] J. Sulc, H. Jelínková, K. Nejezchleb, V. Skoda, Opt. Mater. 30 (2007) 50.
[7] K.S. Lim, C.W. Lee, S.T. Kim, H.J. Seo, C.D. Kim, J. Lumin. 87–89 (2000) 1008.
[8] L.C. Courrol, E.P. Maldonado, L. Gomes, N.D. Vieira, I.M. Ranieri, S.P. Morato, Opt. Mater. 14 (2000) 81.
[9] O. Péron, C. Duverger-Arfuso, Y. Jestin, B. Boulard, M. Ferrari, Opt. Mater. 31 (2009) 1288.
[10] A. Alcalde, A.A. Ribeiro, N.O. Dantas, D.R. Mendes Jr., G.E. Marques, C. Trallero-Giner, Solids 352 (2006) 3618.
[11] N.O. Dantas, F. Qu, R.S. Silva, P.C. Morais, J. Phys. B 106 (2002) 7453.
[12] P.M. Naves, T.N. Gonzaga, A.F.G. Monte, N.O. Dantas, J. Non-Cryst. Solids 352 (2006) 3633.
[13] R.S. Silva, P.C. Morais, A.M. Alcalde, F. Qu, A.F.G. Monte, N.O. Dantas, J. Non-Cryst. Solids 352 (2006) 3522.
[14] N.O. Dantas, E.S.F. Neto, R.S. Silva, D.R. Jesus, F. Pelegrini, Appl. Phys. Lett. 93 (2008) 193115.
[15] R.S. Silva, P.C. Morais, H.S.L. Sullasi, W.E.F. Ayta, F. Qu, N.O. Dantas, IEEE Trans. Magn. 43 (2007) 3124.
[16] N.O. Dantas, R.S. Silva, F. Pelegrini, G.E. Marques, Appl. Phys. Lett. 94 (2009) 263103.
[17] N.O. Dantas, E.O. Serqueira, A.P. Carmo, M.J.V. Bell, V. Anjos, G.E. Marques, Opt. Lett. 35 (2010) 1329.
[18] B.R. Judd, Phys. Rev. 127 (1962) 750.
[19] G.S. Ofelt, J. Chem. Phys. 37 (1962) 511.
[20] A. Majchrowski et al., Mater. Lett. 64 (2010) 295.
[21] A. Agarwal, I. Pal, S. Sanghi, M.P. Aggarwal, Opt. Mater. 32 (2009) 339.
[22] Y. Luo, B. Chen, W. Wu, X. Yu, Q. Yan, Q. Zhang, J. Lumin. 129 (2009) 1309.
[23] W.T. Carnall, P.R. Fields, K. Rajnak, J. Chem. Phys. 49 (1968) 4424.
[24] M. Seshadri, K.V. Rao, J.L. Rao, K.S.R.K. Rao, Y.C. Ratnakaram, J. Lumin. 130 (2010) 536.
[25] K.B. Yatsimirskii, N.K. Davidenko, Coord. Chem. Rev. 27 (1979) 223.
[26] J.H. Choi, A. Margaryan, A. Margaryan, F.G. Shi, J. Lumin. 114 (2005) 167.
[27] Y.C. Ratnakaram, R.P.S. Chakradhar, K.P. Ramesh, J.L. Rao, J. Ramakrishna, J. Phys.: Cond. Matter 15 (2003) 6715.
[28] T. Yamashita, Y. Chishi, J. Appl. Phys. 102 (2007) 123107.
[29] Q. Yanbo et al., J. Rare Earths 24 (2006) 765.
[30] G.N.H. Kumar, J.L. Rao, K.R. Prasad, Y.C. Ratnakaram, J. Alloys Compd. 480 (2009) 208.
[31] Y. Yu, D. Chen, E. Ma, Y. Wang, Z. Hu, Spectrochim. Acta Part A 67 (2007) 709.
[32] C.K. Jorgenson, Modern Aspects of Ligand Field Theory, North Holland, Amsterdam, 1971.
[33] R. Reisfeld, Struct. Bond. 22 (1975) 123.
[34] R. Reisfeld, C.K. Jorgensen, Lasers and Excited States of Rare Earths, Springer-Verlag, Berlin, New York, 1977.
[35] A. Mech, Polyhedron 27 (2008) 393.
[36] A.J. Freeman, R.E. Watson, Phys. Rev. 127 (1962) 2058.
[37] P. Nemec, J. Jedelský, M. Frumar, J. Non-Cryst. Solids 326–327 (2003) 325.
[38] S. Tanabe, J. Non-Cryst. Solids 259 (1999) 1.
[39] A.J.G. Ellison, P.C. Hess, J. Geophys. Res. 95 (1990) 15717.
[40] C.K. Jorgensen, R. Reisfeld, J. Less-Common Metals 93 (1983) 107.
[41] E. Pecoraro, J.A. Sampaio, L.A.O. Nunes, S. Gama, M.L. Baesso, J. Non-Cryst. Solids 277 (2000) 73.
[42] S.E. Stokowski, R.A. Saroyan, M.J. Weber, Lawrence Livermore National Laboratory, M-095, Rev. 2, November, 1981, in: J.F. Michel Digonnet (Ed.), Rare Earth Doped Fiber Lasers and Amplifiers, Marcel Dekker, 47, 1993.
[43] H. Desirena, E. De La Rosa, L.A. Díaz-Torres, G.A. Kumar, Opt. Mater. 28 (2006) 560.
[44] J. Yang, S. Dai, N. Dai, L. Wen, L. Hu, Z. Jiang, J. Lumin. 106 (2004) 9.
[45] S. Xu, Z. Yang, S. Dai, J. Yang, L. Hu, Z. Jiang, J. Alloys Compd. 361 (2003) 313.
[46] Z. Liu, C. Qi, S. Dai, Y. Jiang, L. Hu, Opt. Mater. 21 (2003) 789.
[47] Y. Yan, A.J. Faber, H. Waal, J. Non-Cryst. Solids 181 (1995) 283.
[48] P.M. Peters, S.N. Houde-Walter, J. Non-Cryst. Solids 239 (1998) 162.
[49] Q. Nie, X. Li, S. Dai, T. Xu, Z. Jin, X. Zhang, Spectrochim. Acta Part A 70 (2008) 537.
[50] T. Miyakawa, D.L. Dexter, Phys. Rev. B 1 (1970) 2961.